Energy Storage Materials 16 (2019) 491–497

Contents lists available at ScienceDirect

Energy Storage Materials

journal homepage: www.elsevier.com/locate/ensm

In-situ measurements of stress evolution in composite sulfur cathodes

Yuwei Zhang[a], Yuting Luo[b], Coleman Fincher[a], Scott McProuty[a], Garrett Swenson[a], Sarbajit Banerjee[b], Matt Pharr[a,*]

[a] Department of Mechanical Engineering, Texas A&M University, College Station, TX 77843, USA
[b] Department of Chemistry, Texas A&M University, College Station, TX 77840, USA

ARTICLE INFO

Keywords:
Lithium-sulfur battery
Mechanics
Nucleation and growth
Phase transformations

ABSTRACT

Owing to their enormous capacities, Li-S batteries have emerged as a prime candidate for economic and sustainable energy storage. Still, potential mechanics-based issues exist that must be addressed: lithiation of sulfur produces an enormous volume expansion (~80%). In other high capacity electrodes, large expansions generate considerable stresses that can lead to mechanical damage and capacity fading. However, the mechanics of electrochemical cycling of sulfur is fundamentally distinct from other systems due to solid-to-liquid, liquid-to-liquid, and liquid-to-solid phase transformations, and thus remains poorly understood. To this end, we measure the evolution of stresses in composite sulfur cathodes during electrochemical cycling and link these stresses to structural evolution. We observe that nucleation and growth of solid lithium-sulfur phases induces significant stresses, including irreversible stresses from structural rearrangements during the first cycle. However, subsequent cycles show highly reversible elastic mechanics, thereby demonstrating strong potential for extended cycling in practical applications.

1. Introduction

Battery chemistries beyond lithium-ion are required to meet growing demands for economic and sustainable energy storage/conversion for grid-scale energy storage, portable electronics, and electric vehicles. Sulfur has emerged as a leading candidate to replace conventional cathodes primarily due to its enormous capacity (1672 mAh/g), which is an order of magnitude larger than existing transition-metal cathodes (e.g., 272 mAh/g for $LiCoO_2$) [1–5]. Combined with its abundance in the earth's crust, sulfur cathodes represent a promising low cost, light weight, and sustainable option for the next-generation of battery electrodes [6–11].

Previous studies have implemented a number of *in-situ* techniques to study the electrochemistry and speciation of discharge products in lithium-sulfur batteries, including x-ray absorption near-edge spectroscopy (XANES) [12], electron paramagnetic resonance (EPR) [13], nuclear magnetic resonance (NMR) [14], Raman [15–17], UV/Vis spectroscopy [18,19], x-ray diffraction (XRD) [20–23], and x-ray fluorescence microscopy (XRF) [24]. These studies have elucidated a range of electrochemical issues that cause degradation of the sulfur battery, most notably the shuttling of electrolyte-soluble polysulfides that leads to loss of active material [25–30], the clogging of porous cathode architectures, and the electronically insulating nature of both S and Li_2S that results in poor kinetics and utilization of active material [31–34].

In addition to electrochemical mechanisms of degradation, sulfur cathodes may also be prone to mechanical degradation. In particular, an enormous volume expansion of ~80% accompanies the conversion of S to Li_2S [2,3,5]. Large volume expansions have resulted in mechanical degradation and corresponding capacity losses in many other electrode materials, such as $LiCoO_2$ [35], Si [36–43], Ge [44–46], graphite [47,48], and $LiMn_2O_4$ [49,50], V_2O_5 [51], among others. However, sulfur cathodes exhibit fundamentally distinct behavior in that previously studied electrodes remain in solid form throughout cycling during intercalation or conversion reactions, whereas sulfur undergoes solid-to-liquid, liquid-to-liquid, and liquid-to-solid phase transformations. The influence of such phase transformations on mechanics (e.g., stress levels) is unknown but could be significant given the predicted large volume changes during conversion reactions between S and Li_2S.

To fill these gaps in knowledge, this paper aims to provide fundamental understanding of mechanics in composite sulfur cathodes. To this end, we perform in-situ measurements of mechanical stresses generated during electrochemical cycling of composite sulfur cathodes. Additionally, we correlate these stresses to electrochemical, structural, and phase evolution via combined scanning electron microscopy (SEM), energy dispersive spectroscopy (EDS), and x-ray diffraction (XRD). These efforts offer insight into basic mechanisms underpinning structural changes and their ramifications in terms of

* Corresponding author.
E-mail address: m-pharr@tamu.edu (M. Pharr).

https://doi.org/10.1016/j.ensm.2018.10.001
Received 17 September 2018; Received in revised form 30 September 2018; Accepted 1 October 2018
Available online 04 October 2018
2405-8297/

mechanical degradation during electrochemical cycling of composite sulfur cathodes.

2. Materials and methods

2.1. Cell preparation

We prepared sulfur-carbon composite cathodes through a spin coating process, with compositions of 50 wt% sulfur nanoparticles (99.99% US Research Nanomaterials Inc.) as the active material, 40 wt.% TIMCAL Graphite & Carbon Super P (MTI Corporation) as the matrix, and 10 wt% polyvinylidene fluoride (PVDF, MTI Corporation) as the binder. We created a dispersion of these components in *N*-methyl-2-pyrrolidone (NMP, MTI Corporation), followed by magnetic stirring for 3 h. Lastly, we spin-coated the prepared slurry at 1000 rpm for 1 min onto mirror-finished T304 stainless steel substrates (Metals Depot). After spin coating, we dried the resulting film at 45 °C for 3 h. We used a profilometer (Veeco Dektak 150 Profilometer) to measure the thickness of composite sulfur cathode.

A two-electrode electrochemical test cell with a quartz window (MTI Corporation) facilitated simultaneous electrochemical and mechanical measurements, as depicted in Fig. 1. We assembled this cell in an argon-filled glovebox with oxygen and moisture levels below 0.1 ppm. In addition to the sulfur composite working electrode described above, the battery consisted of a lithium metal ribbon (99.9% trace metals basis, Sigma-Aldrich) anode and a Celgard 2400 separator (MTI Corporation). The electrolyte was 1.0 M lithium *bis*-trifluoromethanesulphonylimide (LiTFSI, Sigma-Aldrich) in (1:1 v/v) 1,3-dioxolane (DOL, Sigma-Aldrich): 1,2-dimethoxyethane (DME, Sigma-Aldrich), with the addition of 0.5 wt% $LiNO_3$ as an additive (Sigma-Aldrich). After assembly, we rested the cell for 8 h prior to electrochemical and mechanical testing to remove the influence of binder swelling on the stress measurements.

2.2. Structural characterization

X-ray diffraction patterns during cycling were collected in a Bragg-Brentano geometry using a Brucker D-8 Discovery diffractometer equipped with a Lynxeye detector (25 kV, 40 mA). After discharging/charging to the desired voltage or state of stress, we disassembled the cells inside the glovebox and washed the sulfur cathodes with anhydrous DME to remove any remaining polysulfides. Since the samples were sensitive to moisture and oxygen, we masked the samples with Kapton™ tape prior to removal from glovebox. A Cu Kα radiation source produced the XRD data, recording between 20 and 35° at a scan rate of 0.0083°s^{-1}.

Scanning electron microscopy (SEM, JEOL JSM-7500F) coupled with energy-dispersive x-ray spectroscopy (EDX, Oxford Instruments) enabled characterizing changes in surface morphology and elemental composition of the sulfur cathodes during cycling. As with the XRD measurements, we cleaned the samples with anhydrous DME prior to examination. Sealing the sample in Static-Shielding Press-to-Close Bags (McMaster-Carr) prevented contamination during transportation to SEM chamber.

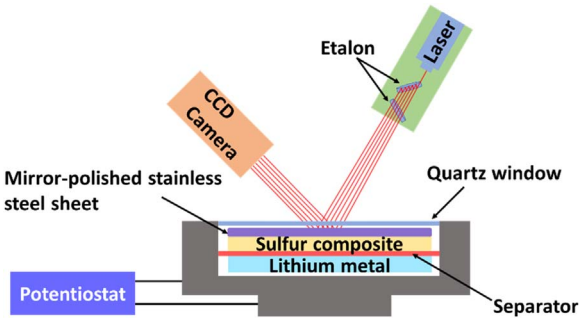

Fig. 1. A schematic representation of the electrochemical setup, using a split cell with a quartz viewing window, in which in-situ multibeam optical sensing enables measurements of stress during electrochemical cycling.

2.3. Electrochemical measurements

Using a PARSTAT MC Multichannel Potentiostat (Princeton Applied Research), we conducted galvanostatic cycling at a C/10 rate between 2.8 V and 1.5 V vs Li/Li^+ [1,2]. The C rate is based on the theoretical capacity of sulfur (1672 mAh/g) [1–3]. All experiments were conducted at room temperature (25 °C).

2.4. Mechanical characterization

A multibeam optical stress sensor (MOS) from k-Space Associates monitored the change in curvature of the sulfur cathode (ΔK) during electrochemical cycling, as shown in Fig. 1. To measure this curvature, the MOS employs an array of laser beams that enables simultaneous illumination and detection, thereby greatly reducing noise caused by fluid motion in the electrochemical cell or by ambient vibrations. The cell was also placed on an antivibration table during testing. To account for the various media through which the laser beam passes in our setup (e.g., the air and quartz window), we calibrated the system using a calibration mirror (radius of curvature of 10 m) inside the electrochemical cell. Using Stoney's equation, we deduced the stress change within the composite cathode during cycling [52,53],

$$\Delta\sigma = \frac{E_s h_s^2}{6h_f(1-\nu_s)}\Delta K,$$

where E_s is the elastic modulus of the substrate, h_s is the thickness of the substrate, ν_s is the Poisson's ratio of the substrate, and h_f is the thickness of electrode film (measured via profilometry before the test). In this study, we take h_f as constant, such that the stress calculated is the nominal in-plane stress. Likewise, previous studies have shown that the thickness change is negligible for porous composite thin films fabricated through slurry deposition methods [47,54–56]. We also measured the thickness change before and after the lithiation, and found the variation to be negligible. Table 1 shows the values of parameters used in the above equation.

3. Results and discussion

3.1. Structural evolution during electrochemical cycling

The cycling curve shown in Fig. 2 highlights the complex compositional changes that occur during the charge/discharge process. Point (a) represents the state of the battery prior to any discharging. Points (b), (d), (f) and (g) are chosen based on notable electrochemical features, while points (c) and (e) are chosen based on mechanical features of interest to be discussed later. This cycling process, involving a series of phase discontinuities, is substantially more complex than found in many other cathode materials, i.e., in many others, simple intercalation/de-intercalation of lithium occurs during cycling [35,47–50,57]. To fully understand this complicated cycling process, we charged/discharged the composite sulfur cathodes to various extents while measuring the evolution of stresses and performed complementary structural characterization using SEM, EDS, and XRD.

Fig. 3 shows SEM images and EDS maps of the surfaces of sulfur

Table 1
Parameters used in stress measurements (Stoney's equation).

E_s (GPa)	h_s (μm)	h_f (μm)	υ_s
203	736	70.3	0.29

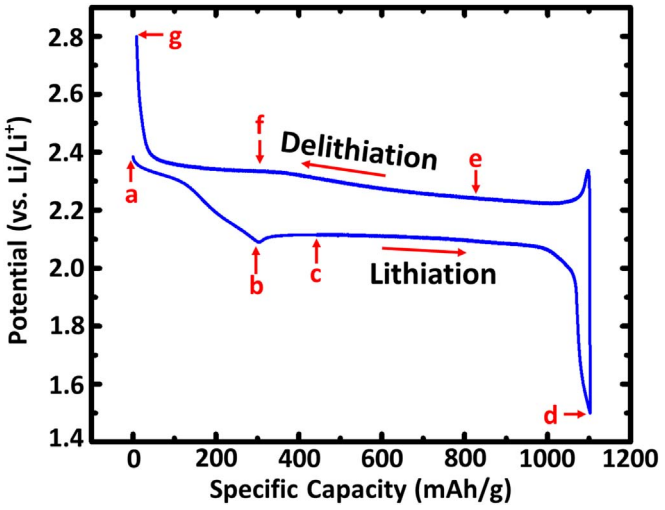

Fig. 2. Representative potential response of a composite sulfur electrode during galvanostatic electrochemical cycling.

composite cathodes charged/discharged to the corresponding labels in Fig. 2. We thoroughly rinsed the samples with dimethyl ether (DME) inside a glovebox prior to analysis by SEM. As a result, the SEM images only show the solid phases. Likewise, Fig. 4 shows the XRD patterns of sulfur composite cathodes charged/discharged to the same extents corresponding to the labels in Fig. 2. From Fig. 3a, the pristine sulfur composite cathode appeared as a near-uniform film composed of a homogeneous mixture of sulfur, carbon, and PVDF. The corresponding XRD pattern at point (a) indicates that sulfur is crystalline orthorhombic α-sulfur prior to lithiation (Fig. 4, label a). As the sulfur converted into electrolyte-soluble polysulfides near the beginning of lower discharge voltage plateau, a substantial portion of the sulfur disappeared, leaving voids within the carbon matrix (Fig. 3b). Correspondingly, the XRD reflections disappeared, indicating the dissolution and electrochemical conversion of sulfur (Fig. 4, label b). With further lithiation, solid products nucleated on the carbon matrix as small islands (Fig. 3c). However, the corresponding XRD reflections provide no evidence of a crystalline phase (Fig. 4, label c). Combining these observations suggests that a solid phase of either Li_2S_2 or Li_2S first formed as an amorphous phase. At the end of lithiation, the surface was almost entirely covered by solid-phase growth products

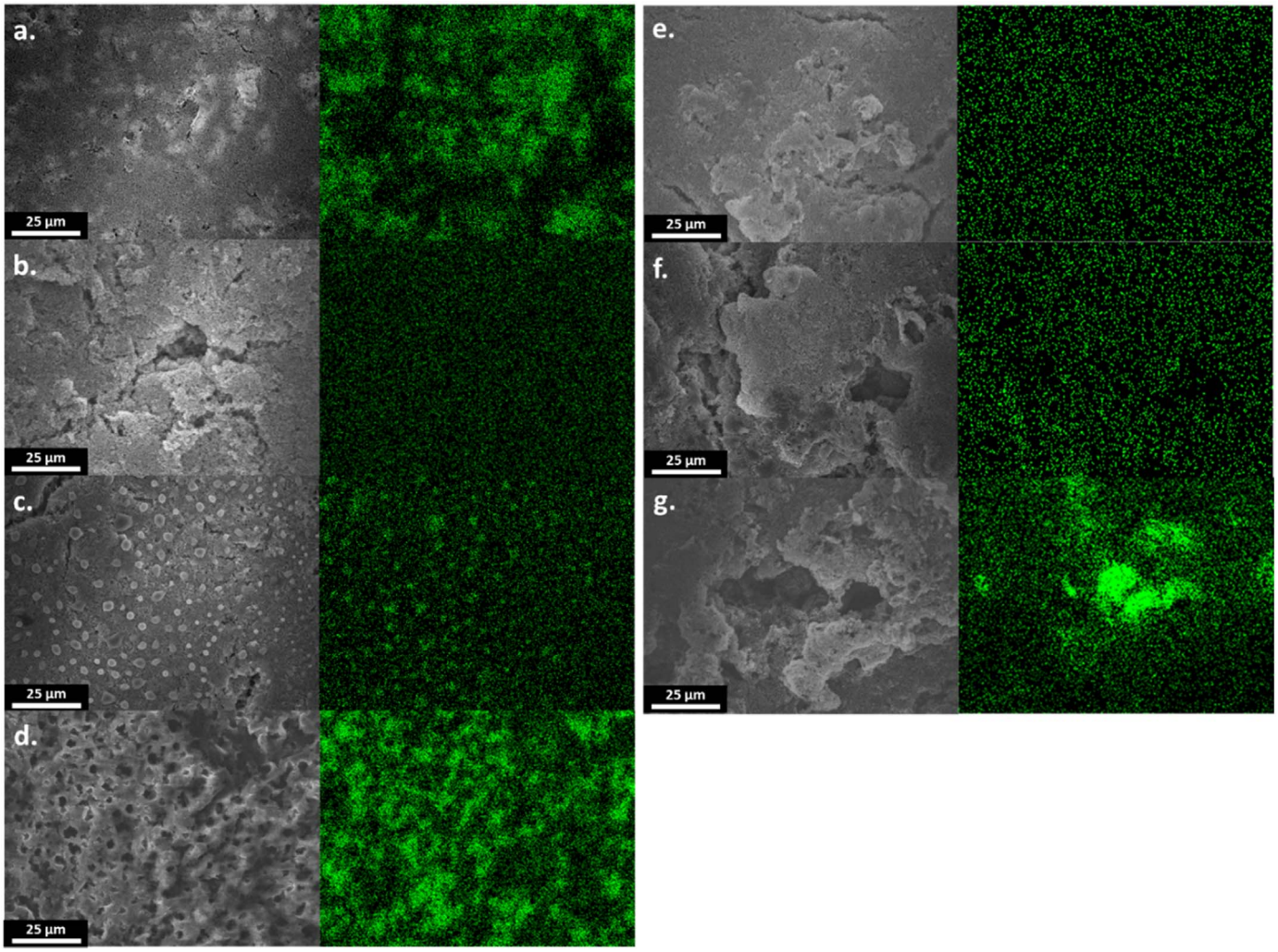

Fig. 3. SEM and EDS images of a sulfur cathode at different states of charge during the first cycle. The green color in the EDS images indicates the presence of sulfur. The letters correspond to the states labeled in Fig. 2, as follows: a) pristine sulfur composite prior to any discharge), b) at the beginning of the lower voltage plateau (2.1 V) during lithiation, c) one special point at the lower voltage plateau during lithiation, d) at the end of lithiation, e) one special point during de-lithiation f) at the beginning of the voltage plateau (2.33 V) during de-lithiation g) at the end of de-lithiation.

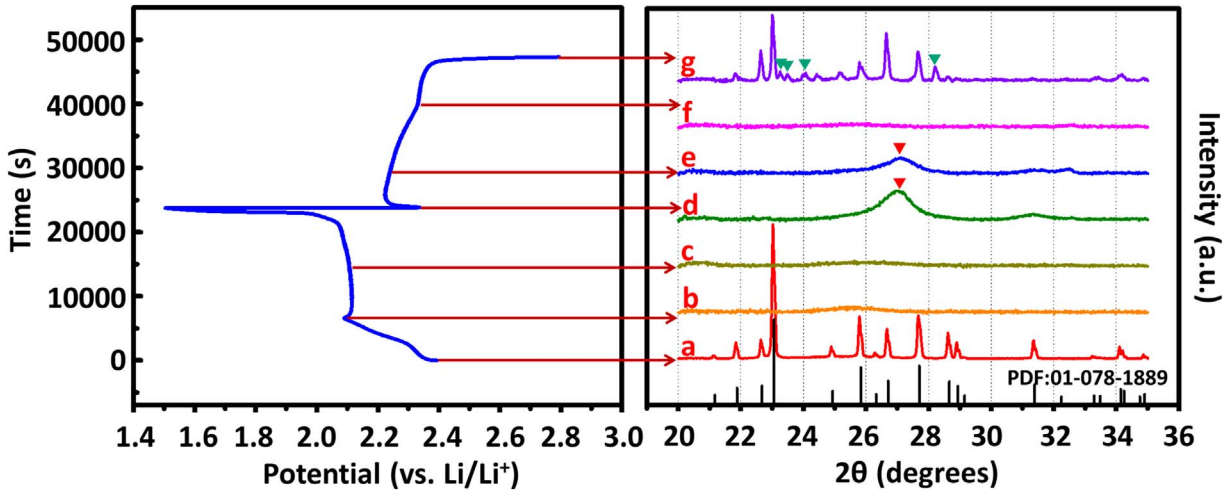

Fig. 4. XRD patterns of a sulfur cathode at different potentials during the first cycle. The red triangles indicate a peak corresponding to Li_2S (PDF number: 00-026-1188). The green triangles indicate peaks corresponding to monoclinic sulfur (β-sulfur) (PDF number: 01-071-0137). The PDF shown in black (PDF number: 01-078-1889) corresponds to orthorhombic sulfur (α-sulfur).

(Fig. 3d), similar to a previous study [58]. The corresponding XRD pattern shows new reflections, which can be indexed to the emergence of crystalline Li_2S (Fig. 4, label d). Overall, these observations indicate that lithiation of sulfur involves dissolution of sulfur into electrolyte-soluble polysulfides, followed by thin film nucleation and growth of solid phases (between points b and d).

Figs. 3e-3g and Figs. 4e-4g show the evolution of the cathode surface and corresponding phase changes during de-lithiation. Between point (d) and (e), the dissolution of the solid lithiated phases began, as indicated by a reduction in the sulfur signal from EDS (Fig. 3e). The intensity of the peak corresponding to crystalline Li_2S concomitantly decreased significantly (Fig. 4, label e), likewise indicating the dissolution of solid crystalline phases. By the time the charging plateau (2.33 V) was reached at point (f), most of the solid lithiated phases had dissolved, and the carbon matrix was clearly visible (Fig. 3f). Moreover, no solid phase of crystalline Li_2S remained according to the XRD results (Fig. 4, label f). At the end of de-lithiation (Fig. 3g), solid sulfur appeared to re-deposit on the matrix, similar to previous studies [22,23,58–60]. At this point, the XRD patterns corresponding to both orthorhombic α-sulfur and monoclinic β-sulfur appeared (Fig. 4, label g), indicating the presence of both polymorphs, consistent with other studies. [21,23] This incipient polymorphism of the deposited sulfur, reflecting the deposition of a metastable phase under conditions away from equilibrium, contributes to the significant difference in morphology before and after the first cycle (Fig. 3a and Fig. 3g).

3.2. Measurements of stress evolution during electrochemical cycling

Fig. 1 shows the experimental setup used to measure stress changes during electrochemical cycling of composite sulfur cathodes. A multi-beam optical stress sensor (MOS) monitored the change in curvature of the sulfur cathode (ΔK) during electrochemical cycling. The results from MOS measurements are shown in Fig. 5a–c. Fig. 5a shows the changes in stress in the sulfur composite cathode during the first five cycles of galvanostatic charge/discharge. We should note that these stresses represent the average stress in the composite film during cycling; they do not provide locally differentiable information (e.g., stress in sulfur *vs*. stress in PVDF). However, these measurements provide useful information regarding the overall mechanics in the system during electrochemical cycling. The stress generated during these five cycles was quite repeatable from cycle to cycle with the exception of the first cycle, i.e., barring the first cycle, features occurred at similar depths of discharge and with similar magnitudes in each cycle. We conducted multiple additional tests to confirm these trends. The first cycle may be different from the others due to the eight-hour resting period, e.g., the upper voltage plateau does not occur during the first cycle as seen in other studies [1–5]. However, this rest period is necessary to ensure that the binder swelling does not contribute significantly to stress measurements, as noted by Sethuraman et al. in a previous study [47]. As a result, binder swelling and/or self-discharge during the resting period may have produced stresses not accounted for here. Correspondingly, the hysteretic change in stress (apparently toward residual tensile stresses) during the first cycle may not be as significant as indicated, as attributed to stress generated during the resting period. Still, our results suggest that hysteretic stresses may occur during the first cycle, likely due to plastic deformation and/or structural evolution (e.g., as in comparing Figs. 3a to 3g).

Additionally, the stresses generated here are substantial but are significantly smaller than those observed in other high-capacity systems, such as Si [42,61] and Ge [45]. These stresses are comparatively small for a number of reasons, due to both the composite nature of this cathode and likely intrinsic to sulfur itself. First, this cathode is a composite that employs relatively compliant binders, which tend to reduce stress levels compared to that intrinsic to the pure active material as has been demonstrated in other systems. For instance, Sethuraman et al. reported the yield stress in a silicon composite anode of 12 MPa (using PVDF as binder), which is approximately 100x smaller than the 1.25 GPa reported for a pure (binder-free) silicon thin film [55,62]. Additionally, composites with relatively compliant binders exhibit low stresses, e.g., as found in comparing the stress levels in a composite silicon anode battery using CMC (70 MPa) and PVDF (12 MPa) as binders [55]. Second, this composite has a porosity of nearly 30%. Thus, stresses are largely accommodated by growth into the pores of the structure, reducing the stresses that are generated, i.e., some stress-free strains occurred. As a result, denser sulfur cathodes will undoubtedly suffer from even larger stresses, which underscores the importance of microstructural/geometric design of sulfur cathodes to prevent mechanical damage. Additionally, these relatively small stresses likely have some contributions from processes intrinsic to sulfur. In particular, lithiation/de-lithiation of sulfur produces solid-to-liquid and liquid-to-solid phase transformations, distinct from other high-capacity systems (e.g., Si [42,61] and Ge [45]). As determined in this study, these solid-to-liquid and liquid-to-solid transformations occur by dissolution and thin film-growth-type-processes, respectively. These types of transformations likely produce intrinsically smaller stresses than occur in systems that undergo purely solid-phase-growth, such as in Si [42,61] and Ge [45].

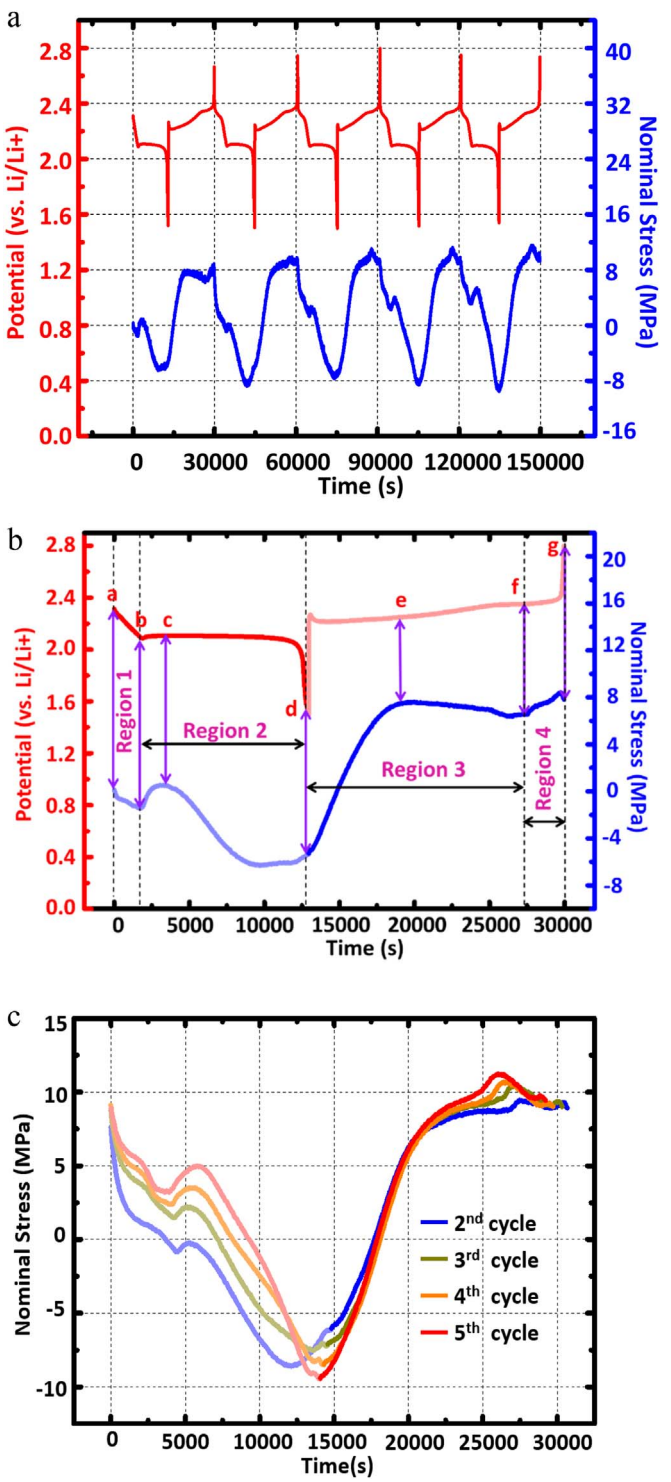

Fig. 5. a. Potential and corresponding stress response during cycling of a composite sulfur cathode. **b**. Potential and corresponding stress response during the initial cycle of a composite sulfur cathode. **c**. Stress response during cycles 2–5 of a composite sulfur cathode.

To further highlight specific details of the mechanics, Fig. 5b displays a zoomed-in view of the stress evolution during the first cycle. The stresses presented represent changes in stress relative to a reference stress, which we take as the stress at the beginning of the first discharge. To reiterate, the upper voltage plateau during lithiation is absent due to self-discharging during the resting period. Thus, along with residual stress in the film from the fabrication process, the choice of reference state may influence the absolute value of the stress. As seen in Fig. 5b, lithiation of the cathode lead to at least two different types of mechanical behavior. In Region 1, the conversion of solid sulfur into liquid polysulfides produced compression relative to our reference state. In this region, the dissolution of solid sulfur removed residual stresses from fabrication and resting (which were apparently tensile here). Next, the stresses generated in Region 2 reflect typical stress evolution during thin film nucleation and growth processes [63–65]. Namely, solid-phase island formation and coalescence (as seen in Fig. 3c) initially induced relative tension between points b and c. As more species were deposited (points c to d), a couple of mechanisms may have contributed to the induced compressive stresses: 1) As Li_xS solids continued to deposit, the inevitable incorporation of atoms from the electrolyte into the interface between solid Li_xS and the carbon matrix created a compressive stress in the film, as observed in lithiation of other battery systems and are typical of thin film growth [42,49,62,66]. 2) Solid-phase conversion of Li_2S_2 to Li_2S was initiated, leading to ~30% volumetric expansion [67]. More specifically regarding (2), SEM and EDS (Fig. 3c) indicate that some kind of solid phase has formed at this depth of discharge, but XRD (Fig. 4, label c) indicates that this phase is amorphous and a clear differentiation between Li_2S_2 or Li_2S is thus not possible. Thus, the increasing compressive stress during the segment (c)-(d) may correlate with the conversion of Li_2S_2 into Li_2S. Lastly, as point (d) was approached, the slope of the stress-vs.-time curve gradually approached zero. If nucleation/growth continued, compressive stresses would likely continue to build up during (c)-(d). We propose two potential mechanisms that may have contributed to the relatively flat curve near the end of lithiation: 1) The driving force for introducing additional excess interface atoms decreased with increasing compressive stresses, eventually producing a steady-state balance. 2) Further lithiation caused plastic yielding in solid lithium sulfide, as has been predicted in simulations [68].

Likewise, de-lithiation also exhibited at least two different types of mechanical behavior. First, in Region 3 the dissolution of solid Li_2S lead to a near-linear relative increase in stress (toward tension) during the segment (d)-(e), which likely represents removal of the stresses that developed during lithiation. After dissolution of the active solid phases, during segment (e)-(f) or Region 3, lower order liquid polysulfides converted to higher order polysulfides, which had little effect on the stress since all of (or the majority of) the phase changes occurred in the liquid state. By comparison, in Region 4, as the higher order polysulfides began to deposit back onto the cathode as crystalline sulfur, relative tensile stresses initially occurred in the cathode (shortly after point (f)), followed by relative compression as the sulfur film was regenerated albeit with a different morphology and phase. In this sense, Region 4 can also be regarded as thin film nucleation and growth process, similar to that of Region 2.

Fig. 5c displays a zoomed-in view of the stress evolution during cycles 2–5. From Fig. 5c, the stresses appeared to behave quite repeatably with further cycling. Several trends appeared here that may have significant implications in practical sulfur systems. First and most importantly, the stress exhibited highly recoverable behavior during the thin film nucleation and growth period of these cycles. That is, while the 1st cycle displayed significant hysteresis, the hysteresis appeared to diminish after the 2nd cycle. An explanation is that the significant stresses generated during the first cycle produced plastic deformation in the form of irreversible structural changes (e.g. α-sulfur changes to a mixture of α-sulfur and β-sulfur at the end of de-lithiation during first cycle as mentioned above) but such structural evolution does not significantly occur thereafter. Second, as a related point, the slope from point e to f (Fig. 5a) is negative (near zero) in cycle 1 while this slope becomes positive in cycles 2–5 (Fig. 5c). Once again, irreversible structural changes that occur during the first cycle likely contribute to this trend (e.g., initially the sample is α sulfur but transforms to α and β sulfur by the end of the first full cycle). Overall, these findings suggest the tantalizing idea that the two polymorphs (α and β) correspond to species favored under different

strain conditions and the mechanical stresses thus direct the phase evolution of the materials [69].

4. Conclusions

In summary, this paper presents the first experimental studies of the mechanical behavior of composite sulfur cathodes during cycling. We observed four major regions of stress generation associated with structural evolution: during discharging: 1) solid-phase conversion of sulfur into electrolyte-soluble polysulfides, followed by 2) deposition of an amorphous solid phase, which ultimately converts to Li_2S, and during charging: 3) dissolution of Li_2S, followed by 4) re-deposition of crystalline sulfur. Different from previously studied intercalative and conversion systems, we conclude that liquid-to-solid phase transformations (nucleation & growth) generate significant stresses during both charging and discharging. Additionally, the measurements indicated that significant hysteresis occurred during the first cycles, which may be attributed to plastic deformation associated with structural transformations. However, subsequent cycles showed nearly elastic and reversible mechanics. As a result, electrodes that withstand the first cycle while retaining active species, which can be engineered through precise mesoscale texturing, hold tremendous promise for structurally robust sulfur-based cathodes. Going forward, we hope our studies will provide fundamental insight into the practical design of mechanically robust sulfur cathodes as well as inspire mechanics-based modeling of coupled electrochemistry, phase transformations, and mechanics.

Declaration of interests

The authors declare no competing interests.

Acknowledgement

Y. Zhang was supported by the Hagler Institute for Advanced Study (HIAS) at Texas A & M University. We thank Huajian Gao for a number of useful discussions pertaining to this work and for his support through the Hagler Institute. C. D. Fincher was supported by the National Science Foundation Graduate Research Fellowship under Grant No. 1746932. Y.Luo and S.Banerjee acknowledge funding from the National Science Foundation under DMR 1809866. M. Pharr acknowledges funding from the mechanical engineering department at Texas A&M University and the Texas A&M Engineering Experiment Station (TEES).

References

[1] H.J. Peng, J.Q. Huang, X.B. Cheng, Q. Zhang, Review on high-loading and high-energy lithium–sulfur batteries, Adv. Energy Mater. 7 (2017) 1–54.
[2] A. Manthiram, Y. Fu, S.H. Chung, C. Zu, Y.S. Su, Rechargeable lithium-sulfur batteries, Chem. Rev. 114 (2014) 11751–11787.
[3] X. Ji, L.F. Nazar, Advances in Li–S batteries, J. Mater. Chem. 20 (2010) 9821.
[4] A. Manthiram, S.-H. Chung, C. Zu, Lithium-sulfur batteries: progress and prospects, Adv. Mater. 27 (2015) 1980–2006.
[5] Z.W. Seh, Y. Sun, Q. Zhang, Y. Cui, Designing high-energy lithium–sulfur batteries, Chem. Soc. Rev. 45 (2016) 5605–5634.
[6] M.-K. Song, E.J. Cairns, Y. Zhang, Lithium/sulfur batteries with high specific energy: old challenges and new opportunities, Nanoscale 5 (2013) 2186.
[7] Y.X. Yin, S. Xin, Y.G. Guo, L.J. Wan, Lithium-sulfur batteries: electrochemistry, materials, and prospects, Angew. Chemie - Int. Ed. (2013) 13186–13200.
[8] S. Xin, et al., Smaller sulfur molecules promise better lithium'sulfur batteries, J. Am. Chem. Soc. 134 (2012) 18510–18513.
[9] L. Yuan, H. Yuan, X. Qiu, L. Chen, W. Zhu, Improvement of cycle property of sulfur-coated multi-walled carbon nanotubes composite cathode for lithium/sulfur batteries, J. Power Sources 189 (2009) 1141–1146.
[10] Y. Yue, H. Liang, 3D Current Collectors for Lithium-Ion Batteries: A Topical Review. 1800056, 2018, pp. 1–20.
[11] X. Pu, G. Yang, C. Yu, Liquid-type cathode enabled by 3D sponge-like carbon nanotubes for high energy density and long cycling life of Li-S Batteries, Adv. Mater. 26 (2014) 7456–7461.
[12] M. Cuisinier, et al., Sulfur speciation in Li-S batteries determined by operando X-ray absorption spectroscopy, J. Phys. Chem. Lett. 4 (2013) 3227–3232.
[13] Q. Wang, et al., Direct observation of sulfur radicals as reaction media in lithium sulfur batteries, J. Electrochem. Soc. 162 (2015) A474–A478.
[14] J. Xiao, et al., Following the transient reactions in lithium-sulfur batteries using an in situ nuclear magnetic resonance technique, Nano Lett. 15 (2015) 3309–3316.
[15] M. Hagen, et al., In-situ Raman investigation of polysulfide formation in Li-S cells, J. Electrochem. Soc. 160 (2013) A1205–A1214.
[16] J.-T. Yeon, et al., Raman spectroscopic and X-ray diffraction studies of sulfur composite electrodes during discharge and charge, J. Electrochem. Soc. 159 (2012) A1308–A1314.
[17] H.L. Wu, L.A. Huff, A.A. Gewirth, In situ raman spectroscopy of sulfur speciation in lithium-sulfur batteries, ACS Appl. Mater. Interfaces 7 (2015) 1709–1719.
[18] M.U.M. Patel, et al., Li-S battery analyzed by UV/vis in operando mode, ChemSusChem 6 (2013) 1177–1181.
[19] Q. Zou, Y.C. Lu, Solvent-dictated lithium sulfur redox reactions: an operando UV–vis spectroscopic study, J. Phys. Chem. Lett. 7 (2016) 1518–1525.
[20] J. Conder, et al., Direct observation of lithium polysulfides in lithium-sulfur batteries using operando X-ray diffraction, Nat. Energy 2 (2017) 1–7.
[21] S. Waluś, et al., New insight into the working mechanism of lithium–sulfur batteries: in situ and operando X-ray diffraction characterization, Chem. Commun. 49 (2013) 7899.
[22] J. Nelson, et al., In operando X-ray diffraction and transmission X-ray microscopy of lithium sulfur batteries, J. Am. Chem. Soc. 134 (2012) 6337–6343.
[23] W. Zhu, et al., Investigation of the reaction mechanism of lithium sulfur batteries in different electrolyte systems by in situ Raman spectroscopy and in situ X-ray diffraction, Sustain. Energy Fuels 1 (2017) 737–747.
[24] X. Yu, et al., Direct observation of the redistribution of sulfur and polysufides in Li-S batteries during the first cycle by in situ X-ray fluorescence microscopy, Adv. Energy Mater. 5 (2015) 1–6.
[25] E.P. Kamphaus, P.B. Balbuena, First-principles investigation of lithium polysulfide structure and behavior in solution, J. Phys. Chem. C 121 (2017) 21105–21117.
[26] H. Wang, et al., Graphene-wrapped sulfur particles as a rechargeable lithium-sulfur battery cathode material with high capacity and cycling stability, Nano Lett. 11 (2011) 2644–2647.
[27] X. Ji, K.T. Lee, L.F. Nazar, A highly ordered nanostructured carbon-sulphur cathode for lithium-sulphur batteries, Nat. Mater. 8 (2009) 500–506.
[28] Y.V. Mikhaylik, J.R. Akridge, Polysulfide shuttle study in the Li/S battery system, J. Electrochem. Soc. 151 (2004) A1969.
[29] G. Zheng, Y. Yang, J.J. Cha, S.S. Hong, Y. Cui, Hollow carbon nanofiber-encapsulated sulfur cathodes for high specific capacity rechargeable lithium batteries, Nano Lett. 11 (2011) 4462–4467.
[30] D.S. Wu, et al., Quantitative investigation of polysulfide adsorption capability of candidate materials for Li-S batteries, Energy Storage Mater. 13 (2018) 241–246.
[31] Y. Yang, G. Zheng, Y. Cui, Nanostructured sulfur cathodes, Chem. Soc. Rev. 42 (2013) 3018.
[32] G. He, X. Ji, L. Nazar, High "C" rate Li-S cathodes: sulfur imbibed bimodal porous carbons, Energy Environ. Sci. 4 (2011) 2878.
[33] Z. Liu, P.B. Balbuena, P.P. Mukherjee, Revealing charge transport mechanisms in Li_2S_2 for Li–sulfur batteries, J. Phys. Chem. Lett. 8 (2017) 1324–1330.
[34] J. Schuster, et al., Spherical ordered mesoporous carbon nanoparticles with high porosity for lithium-sulfur batteries, Angew. Chem. 124 (2012) 3651–3655.
[35] K. Zhao, M. Pharr, J.J. Vlassak, Z. Suo, Fracture of electrodes in lithium-ion batteries caused by fast charging, J. Appl. Phys. 108 (2010) 1–7.
[36] K. Zhao, M. Pharr, L. Hartle, J.J. Vlassak, Z. Suo, Fracture and debonding in lithium-ion batteries with electrodes of hollow core-shell nanostructures, J. Power Sources 218 (2012) 6–14.
[37] G.R. Hardin, Y. Zhang, C.D. Fincher, M. Pharr, Interfacial fracture of nanowire electrodes of lithium-ion batteries, JOM 69 (2017) 1519–1523.
[38] M.T. McDowell, et al., Studying the kinetics of crystalline silicon nanoparticle lithiation with in situ transmission electron microscopy, Adv. Mater. 24 (2012) 6034–6041.
[39] K. Zhao, et al., Concurrent reaction and plasticity during initial lithiation of crystalline silicon in lithium-ion batteries, J. Electrochem. Soc. 159 (2012) A238–A243.
[40] I. Ryu, J.W. Choi, Y. Cui, W.D. Nix, Size-dependent fracture of Si nanowire battery anodes, J. Mech. Phys. Solids . 59 (2011) 1717–1730.
[41] X.H. Liu, et al., Size-dependent fracture of silicon nanoparticles during lithiation, ACS Nano 6 (2012) 1522–1531.
[42] M. Pharr, Z. Suo, J.J. Vlassak, Measurements of the fracture energy of lithiated silicon electrodes of Li-Ion batteries, Nano Lett. 13 (2013) 5570–5577.
[43] S.T. Boles, C.V. Thompson, O. Kraft, R. Mönig, In situ tensile and creep testing of lithiated silicon nanowires, Appl. Phys. Lett. 103 (2013) 1–5.
[44] X. Wang, A. Yang, S. Xia, Fracture toughness characterization of lithiated germanium as an anode material for lithium-ion batteries, J. Electrochem. Soc. 163 (2016) A90–A95.
[45] M. Pharr, Y.S. Choi, D. Lee, K.H. Oh, J.J. Vlassak, Measurements of stress and fracture in germanium electrodes of lithium-ion batteries during electrochemical lithiation and delithiation, J. Power Sources 304 (2016) 164–169.
[46] A. Al-Obeidi, D. Kramer, C.V. Thompson, R. Mönig, Mechanical stresses and morphology evolution in germanium thin film electrodes during lithiation and delithiation, J. Power Sources 297 (2015) 472–480.
[47] V.A. Sethuraman, N. Van Winkle, D.P. Abraham, A.F. Bower, P.R. Guduru, Real-time stress measurements in lithium-ion battery negative-electrodes, J. Power Sources 206 (2012) 334–342.
[48] A. Mukhopadhyay, A. Tokranov, X. Xiao, B.W. Sheldon, Stress development due to surface processes in graphite electrodes for Li-ion batteries: a first report, Electrochim. Acta 66 (2012) 28–37.

[49] J. Sheth, et al., In situ stress evolution in Li $_{1+x}$ Mn $_{2}$ O $_{4}$ thin films during electrochemical cycling in Li-ion cells, J. Electrochem. Soc. 163 (2016) A2524–A2530.
[50] W.H. Woodford, Y.-M. Chiang, W.C. Carter, “Electrochemical Shock” of intercalation electrodes: a fracture mechanics analysis, J. Electrochem. Soc. 157 (2010) A1052.
[51] Y. Luo, et al., Roadblocks in cation diffusion pathways: implications of phase boundaries for Li-ion diffusivity in an intercalation cathode material, ACS Appl. Mater. Interfaces (2018). http://dx.doi.org/10.1021/acsami.8b10604 (acsami.8b10604).
[52] G.G. Stoney, The tension of metallic films deposited by electrolysis, Proc. R. Soc. A Math. Phys. Eng. Sci. 82 (1909) 172–175.
[53] W.D. Nix, Mechanical properties of thin films, Metall. Trans. A 20 (1989) 2217–2245.
[54] R. Kumar, J.H. Woo, X. Xiao, B.W. Sheldon, Internal microstructural changes and stress evolution in silicon nanoparticle based composite electrodes, J. Electrochem. Soc. 164 (2017) A3750–A3765.
[55] S.P.V. Nadimpalli, V.A. Sethuraman, D.P. Abraham, A.F. Bower, P.R. Guduru, Stress evolution in lithium-ion composite electrodes during electrochemical cycling and resulting internal pressures on the cell casing, J. Electrochem. Soc. 162 (2015) A2656–A2663.
[56] V.A. Sethuraman, et al., Stress evolution in composite silicon electrodes during lithiation/delithiation, J. Electrochem. Soc. 160 (2013) A739–A746.
[57] Z. Qi, et al., LiNi0.5Mn0.3Co0.2O2/Au nanocomposite thin film cathode with enhanced electrochemical properties, Nano Energy 46 (2018) 290–296.
[58] S. Waluš, et al., Lithium/sulfur batteries upon cycling: structural modifications and species quantification by in situ and operando X-ray diffraction spectroscopy, Adv. Energy Mater. 5 (2015) 1–5.
[59] Y. Wang, et al., Structural change of the porous sulfur cathode using gelatin as a binder during discharge and charge, Electrochim. Acta 54 (2009) 4062–4066.
[60] S. Xiong, K. Xie, Y. Diao, X. Hong, Oxidation process of polysulfides in charge process for lithium-sulfur batteries, Ionics 18 (2012) 867–872.
[61] M. Pharr, Z. Suo, J.J. Vlassak, Variation of stress with charging rate due to strain-rate sensitivity of silicon electrodes of Li-ion batteries, J. Power Sources 270 (2014) 569–575.
[62] V.A. Sethuraman, M.J. Chon, M. Shimshak, V. Srinivasan, P.R. Guduru, In situ measurements of stress evolution in silicon thin films during electrochemical lithiation and delithiation, J. Power Sources 195 (2010) 5062–5066.
[63] R.C. Cammarata, T.M. Trimble, Surface stress model for intrinsic stresses in thin films, J. Mater. Res. 15 (2000) 2468–2474.
[64] A.L. Del Vecchio, F. Spaepen, The effect of deposition rate on the intrinsic stress in copper and silver thin films, J. Appl. Phys. 101 (2007).
[65] H. Windischmann, Intrinsic stress in sputtered thin films, J. Vac. Sci. Technol. A Vac. Surf. Film 9 (1991) 2431–2436.
[66] L. FreundS. Suresh, Thin Film Materials: Stress, Defect Formation and Surface Evolution, 768, 2003. ⟨http://dx.doi.org/10.1017/CBO9780511754715⟩.
[67] Z. Feng, et al., Unravelling the role of Li2S2in lithium-sulfur batteries: a first principles study of its energetic and electronic properties, J. Power Sources 272 (2014) 518–521.
[68] M. Wang, J. Yu, S. Lin, Lithiation-assisted strengthening effect and reactive flow in bulk and nanoconfined sulfur cathodes of lithium-sulfur batteries, J. Phys. Chem. C 121 (2017) 17029–17037.
[69] A. Parija, G.R. Waetzig, J.L. Andrews, S. Banerjee, Traversing energy landscapes away from equilibrium: strategies for accessing and utilizing metastable phase space, J. Phys. Chem. C (2018). http://dx.doi.org/10.1021/acs.jpcc.8b04622.